



1 What is climate change doing in Himalaya? Thirty 2 years of the Pyramid Meteorological Network (Nepal)

3 Franco Salerno^{1,2,*†}, Nicolas Guyennon^{3,**†}, Nicola Colombo⁴, Maria Teresa Melis^{5,6},
4 Francesco Gabriele Dessì⁵, Gianpietro Verza⁵, Kaji Bista⁷, Ahmad Sheharyar¹, Gianni
5 Tartari²

- 6
7 1 National Research Council, Institute of Polar Sciences, ISP-CNR, Milan, Italy
8 2 National Research Council, Water Research Institute, IRSA-CNR, Brughiero (MB), Italy;
9 3 National Research Council, Water Research Institute, IRSA-CNR, Montelibretti (Roma), Italy;
10 4 Department of Agricultural, Forest and Food Sciences, University of Turin, Grugliasco, Italy
11 5 Ev-K2-CNR, Bergamo, Italy;
12 6 Dipartimento of Chemical and Geological Sciences, University of Cagliari, Monserrato (CA), Italy
13 7 Nepal Academy of Science and Technology (NAST), Kathmandu, Nepal

14
15 * Correspondence: franco.salerno@cnr.it; **nicolas.guyennon@irsa.cnr.it
16 † Franco Salerno and Nicolas Guyennon equally contributed to this paper.

17

18 Abstract

19 Climate change is deeply impacting mountain areas around the globe, especially in
20 Himalaya. However, the lack of long-term meteorological observations at high elevations
21 poses significant challenges to understand and predict impacts at various scales. This also
22 represents a serious limit for model-based projections of future behavior of crucial
23 elements of the mountain cryosphere such as glaciers. Here, we present the Pyramid
24 Meteorological Network, located in Himalaya (Nepal), on the southern slopes of Mt.
25 Everest. The network is composed of 7 meteorological stations located between 2660 and
26 7986 m a.s.l., which have collected continuous climatic data during the last 30 years
27 (1994-2023). In this paper, details are provided regarding instrument types and
28 characteristics as well as data quality control and assessment. The obtained data series are
29 available on a newly created geportal. We leverage these unique records to present new
30 knowledge on the Himalayan climate, benefiting also from the highest observational
31 climatic series in the world (Pyramid station, located at above 5000 m a.s.l., close to
32 Khumbu Glacier). These data will provide fundamental knowledge on climate dynamics
33 in Himalaya that will inform research at high elevations in the coming years. The dataset



34 is available freely accessible from <https://geoportal.mountaingenius.org/portal/>
35 (<https://zenodo.org/records/14450214>) (Salerno et al., 2024).

36 1 Introduction

37 Global temperature has been increasing at unprecedented rates during the Anthropo-
38 cene, impacting both natural and human systems (e.g., Mukherji et al., 2023). Alpine bi-
39 oomes, among the most sensitive natural ecosystems to climate warming, show rapid shifts
40 of species distribution ranges and modulations of species interactions (e.g., Sigdel et al.,
41 2021). Himalayan glaciers have been losing mass in the last decades (Biemans et al.,
42 2019). The current uncertainties concerning the glacial shrinkage in the Himalayas are
43 mainly attributed to the lack of measurements of climatic forcings (e.g., Bhattacharya at
44 al., 2021). Indeed, recent research has underlined the need for fine scale investigations,
45 especially at high elevation, to better model the glacio-hydrological dynamics (Yao et al.,
46 2022). In addition, according to Yang et al. (2018), reliable meteorological data at glacial
47 elevations are essential to: (1) place the observed glacial changes in the context of current
48 climatic change, (2) understand hydro-meteorological relationships in cryospheric envi-
49 ronments, and (3) calibrate dynamically and statistically downscaled climate fields. How-
50 ever, there are few high-elevation weather stations where the glaciers are located, espe-
51 cially in Himalaya. This can be attributed to the remote location of glaciers and the rugged
52 terrain, which make physical access difficult (e.g., Salerno et al., 2015; Lin et al., 2021).

53 As a consequence of the remoteness and difficulty in accessing several high-elevation
54 sites combined with the complications of operating automated weather stations (AWSs)
55 in remote areas, long-term measurements are challenging (Yang et al., 2018). For in-
56 stance, in Himalaya, meteorological stations at high elevations are extremely scarce
57 (Mountain Research Initiative EDW Working Group, 2015; Salerno et al., 2015; T. Mat-
58 thews et al., 2020). Therefore, in several studies, climatic data at high elevations had to
59 be estimated using low-elevation data (Shrestha et al., 2014; Zhang et al., 2015), which
60 are more common. This is the case of the central Himalaya, where the Department of
61 Hydrology and Meteorology of Nepal (www.dhm.gov.np/) maintains more than 300 long-
62 term rain stations, although they are mainly located below 3000 m a.s.l..

63 In this context, in the early 1990s, the Pyramid Meteorological Network was created
64 by the Italian *Ev-K2-CNR Committee* (www.ev-k2-cnr.org). This network is composed of



65 7 automatic weather stations located on the southern side of Mt Everest (along the
66 Khumbu Valley), in the central Himalaya (Sagarmatha National Park - SNP; Amatya et
67 al., 2010; Salerno et al., 2010) ranging from 2660 to 7986 m a.s.l.. For each station, the
68 following variables are collected on an hourly basis: air temperature, total precipitation,
69 relative humidity, atmospheric pressure, and wind speed and direction.

70 Here, we present the database in which all meteorological data are stored, freely ac-
71 cessible from <https://geoportal.mountaingenius.org/portal/> (<https://zenodo.org/records/14450214>), and we explore the small-scale climate variability of the longest time
72 series of the network, the Pyramid station (5035 m a.s.l.), located close to the Khumbu
73 Glacier.
74

75

76 **2 Region of investigation**

77 Salerno et al., 2015 describes the ground network of automatic weather stations
78 (AWSs) belongs to the Pyramid Meteorological Network, which is located on the
79 southern side of Mt Everest (along the Khumbu Valley), in central Himalaya (Sagarmatha
80 National Park - SNP; Amatya et al., 2010; Salerno et al., 2010) (Fig. 1). The land-cover
81 classification shows that almost one-third of the territory is characterised by glaciers and
82 ice cover, while less than 10% of the park area is forested (*Abies spectabilis*, *Betula utilis*)
83 (Magnani et al., 2018; Pandey et al., 2020). The tree line is located at approx. 4050 m
84 a.s.l., while the landscape is dominated by alpine tundra and lichen above this elevation
85 (Bhujju et al., 2010; Sigdel et al., 2021). Glacial surfaces are distributed from 4300 to
86 above 8000 m a.s.l. Around 75% of the glacier surfaces are located between 5000 and
87 6500 m a.s.l. (Thakuri et al., 2014, 2016), and ca. 25% of the glacierised area is debris-
88 covered (Shea et al., 2015; Salerno et al., 2017). Glaciers in this area are classified as the
89 summer-accumulation type, which are fed mainly by summer monsoon precipitation
90 (Tartari et al., 2008).

91 The climate in the South Asia and Himalayan region has a strong annual cycle, with
92 the South Asian monsoon that is a phase of this annual cycle. During the pre-monsoon
93 season (MAM), the westerlies prevail over this region and are deflected when crossing
94 the Himalayan mountains. During the monsoon season (JJAS), the westerlies move
95 northward, while south-westerly flows dominate the upper level and southeasterly flows
96 from Bay of Bengal dominates the lower level (Ichiyonagi et al., 2007). After the offset



97 of the monsoon, the south-westerly and southeasterly flows are replaced by the westerlies.
98 The warm area moves to the south and both air temperature and humidity decrease
99 considerably. Cooling and drying are further enhanced towards the winter (Yang et al.,
100 2018).

101 Regarding the precipitation, the measurements at Pyramid station (Z5035) show that
102 90% is concentrated from June to September, while the probability of snowfall during
103 these months is very low (4%); the annual cumulated precipitation at this elevation is 446
104 mm, with a mean annual temperature of -2.5 °C (Salerno et al., 2015). Precipitation
105 linearly increases to an elevation of 2500 m a.s.l. and exponentially decreases at higher
106 elevations (Salerno et al., 2015). Finally, the wind regime of the area is characterised by
107 up-valley winds during the day throughout the year, while weak up-valley winds occur at
108 night during the monsoon season, with some evidence of down-valley winds occurring at
109 night in the winter (Potter et al., 2018 and references therein reported). Strong diurnal
110 katabatic winds also occur at the higher elevations (above ca. 4500 m a.s.l.) due to
111 enhanced glacier melting under warm atmospheric conditions (Salerno, et al., 2023).

112 **3 Data and methods**

113 **3.1 Weather stations**

114 The first automatic weather station (AWS0) was installed in October 1993, near the
115 Pyramid Laboratory, at 5035 m a.s.l. (Fig. 1, 2; Bertolani et al., 2000). AWS0 recorded
116 temperature data until December 2005. A new station (AWS1) was installed just a few
117 tens of meters away from AWS0 and it has been operating since October 2000. The other
118 stations were installed in the following years in the Khumbu Valley (Fig. 1, Tab. 1). In
119 2008, the network included seven monitoring sites, including the highest weather station
120 of the world, located at South Col of Mt. Everest (7986 m a.s.l.). The locations of all
121 stations are presented in Figure 1, while Figure 3 shows the temporal availability of the
122 meteorological data. AWS3 (Z2660) and AWS5 (Z3570) are located below the tree line,
123 while AWS2 (Z4260) is located close to the upper limit of the vegetation. At higher ele-
124 vation, AWS0 and AWS1 (Z5035) are close to the glacier front elevation, AWS4 (Z5600)
125 is situated at the mean elevation of glaciers, and AWSCC (Z7986) characterises the high-
126 est peaks. The list of measured variables, sensors, manufacturer and accuracy for each
127 station is presented in Table 3.



128 Recently, a new meteorological network was established in the Khumbu Valley by the
129 2019 National Geographic and Rolex Everest Expedition
130 (<https://datadash.appstate.edu/high-altitude-climate/#download>), with 5 stations ranging
131 from 3810 to 8430 m a.s.l. (Matthews et al., 2020). On average, this network is located at
132 an elevation higher than the Pyramid Meteorological Network, representing mainly the
133 accumulation zone of the glaciers in the region. Moreover, the GLACIOCLIM group
134 manages some stations on Changri Nup and Mera Glacier (Wagnon et al., 2021).

135

136 **3.2 Geoportal structure**

137 Since the early 1990s, when the Pyramid Meteorological Network was created, the Ev-
138 K2-CNR Committee has promoted the sharing of data collected from high-elevation
139 AWSs. In 2014, the first data sharing system was born, and it was called SHARE (Station
140 at High Altitude for Research on the Environment) Geonetwork. The system collected
141 data from 15 stations spread across four countries (Nepal, Pakistan, Italy, and Uganda).
142 The system was designed for open data management, in line with international directives
143 and standards for free access to environmental data. Furthermore, based on a
144 customisation of the GeoNetwork software system, a hierarchical database of the
145 individual stations and sensors was created (Melis et al., 2013; Locci et al., 2014).

146 In the last ten years, this web platform has been improved according to new digital
147 standards and software release. Furthermore, the publication of station data was
148 accompanied by a new web-GIS platform to provide three services: 1) a structured
149 metadata and data archive, 2) a simplified interface to provide access to AWSs' data, and
150 3) a dedicated webGIS platform for geo-referenced data. The new GeoPortal is accessible
151 at the address <https://geoportal.mountaingenius.org/portal/>.

152 An exclusive function provided by the GeoPortal is the direct access to dataset and
153 databases through a dedicated search data-tab in the portal main menu. Dataset acquired
154 by the projects are stored in a PostgreSQL DBMS: registered GeoPortal users can query
155 the data by the Search Data command, and in the results page, it is possible to proceed to
156 direct download dataset in csv format or to directly consult them in forms of tables and
157 charts. All information provided by the portal is supplied with their relative metadata. The
158 metadata database is the core of system: only through metadata it is possible to search
159 and retrieve resources. The main search window allows to search any string occurrence



160 in the metadata database: through the result page it is possible to access directly to the
161 metadata sheet with description of resource. Here it is possible to retrieve the direct
162 connection with dataset with the possibility of a direct download of the supplied dataset,
163 accordingly with the file format. Metadata and datasets are strictly related with a two-
164 ways connection.

165

166 **3.3 Data gap filling for temperature and precipitation time series**

167 Pyramid station has suffered a percentage of missing daily values of ca. 10% and
168 15% for temperature and precipitation, respectively (Table 2). In this study, we applied
169 the same gap filling method (quantile mapping) used for missing data in Salerno et al.
170 (2015), but extending the time series to 2023. All the stations belonging to the network
171 were tested and used for filling the gaps according to a priority criterion based on the
172 degree of correlation among data. AWS1 was chosen as the reference station given the
173 length of the time series and the fact that it is currently still operating. The selected filling
174 method is a simple regression analysis based on quantile mapping (e.g., Déqué, 2007;
175 Themeßl et al., 2012). This regression method has been preferred to more complex
176 techniques, such as the fuzzy rule-based approach (Abebe et al., 2000) or the artificial
177 neural networks (Abudu et al., 2010; Coulibaly and Evora, 2007), considering the
178 peculiarity of this case study where all stations are located in the same valley (Khumbu
179 Valley). This aspect confines the variance among the stations to the elevational gradient
180 of the considered variable, which can be easily reproduced by the stochastic link created
181 by the quantile mapping method. In case all stations registered a simultaneous gap, we
182 applied a multiple imputation technique (Schneider, 2001) that uses some other proxy
183 variables to fill the remaining missing data. The uncertainty introduced by the filling
184 process on the Sen's slope (SS) was estimated through a Monte Carlo uncertainty
185 analysis. Details on the reconstruction procedure and the computation of the associated
186 uncertainty are provided in Salerno et al. (2015).

187 **3.4 Statistical analysis**

188 In this study, the Mann–Kendall test (MK, Kendall, 1975) was applied at the
189 monthly scale (after daily data aggregation) to analyse the non-stationarity of meteorological
190 data. This test is widely adopted to assess significant trends in



191 hydrometeorological time series (Guyennon et al., 2013). This test is non-parametric, thus
192 being less sensitive to extreme sample values and is independent from the hypothesis
193 about the nature of the trend, whether linear or not. The MK test verifies the assumption
194 of the stationarity of the investigated series by ensuring that the associated normalized
195 Kendall's tau-b coefficient, $\mu(\tau)$, is included within the confidence interval for a given
196 significance level (for $\alpha = 5\%$, the $\mu(\tau)$ is below -1.96 and above 1.96). We used the Sen's
197 slope (SS) proposed by Sen (1968) as a robust linear regression allowing the quantifica-
198 tion of the potential trends revealed by the MK. The significance level is established for
199 $P < 0.05$. We defined a slight significance for $P < 0.10$. The uncertainty associated with
200 the SS (1994–2013) is estimated through a Monte Carlo uncertainty analysis (James and
201 Oldenburg, 1997). In the sequential form (seqMK) $\mu(\tau)$ the test is applied forward starting
202 from the oldest values (progressive trend) and backward starting from the most recent
203 values (retrograde trend). The crossing period allows us to identify the approximate start-
204 ing point of the trend. In this study, the seqMK is applied to monthly vectors. Monitoring
205 the seasonal non-stationarity, the monthly progressive $\mu(\tau)$ is reported with a pseudo
206 color code, where the warm colors represent the positive slopes and cold colors the neg-
207 ative ones

208 **4 Results and discussion**

209 At 5035 m a.s.l., the precipitation is concentrated during June–September (around
210 90%, Fig. 4) and, considering that the mean daily temperature during these months is
211 above $+0^\circ\text{C}$, we can infer that during these months the probability of snowfall is very
212 low. According to Salerno et al. (2015), the underestimation of precipitation fallen as
213 snow during the other months should not be over 20%. Sustained by this analysis, the
214 trend analysis of precipitation was focused to the warmest months (Fig. 5d).

215 Trend analysis at high elevation

216 Figure 5 shows the reconstructed Pyramid time series for Tmin, Tmax, Tmean, and
217 Prec, after the gap filling procedure. These daily time series for the 1994–2023 period are
218 available at <https://geoportal.mountaingenius.org/portal/>. These data, until 2020, have
219 been presented in Salerno et al. (2023). In this paper, the last three years have been added
220 to the time series and now we present the results of the last 30 years (1994–2023).



221 *Maximum air temperature (Tmax)*

222 During the warm season (from May to October), Tmax shows a significant negative
223 trend ($-0.31 \pm 0.015 \text{ } ^\circ\text{C y}^{-1}$, $p < 0.05$) as highlighted by the progressive $\mu(\tau)$ trend in
224 the bottom graph (full line in orange, Fig. 5a). Increases (although not significant) are
225 observed in November and December; generally, the cold season (from November to
226 April) shows no trend ($-0.006 \pm 0.013 \text{ } ^\circ\text{C y}^{-1}$, $p > 0.1$) (full line in blue). On the annual
227 scale the trend is negative, but not significant ($-0.022 \pm 0.011 \text{ } ^\circ\text{C y}^{-1}$, $p > 0.1$). The
228 decreasing trend seems to have started in 2007 for the warm season, while in the previous
229 years the negative trend was restricted to only MJJ months, whereas the cold months
230 shows a later start of the decreasing trend, i.e. from 2011.

231 *Minimum air temperature (Tmin)*

232 November ($+0.06 \text{ } ^\circ\text{C y}^{-1}$, $p < 0.05$) and December ($+0.08 \text{ } ^\circ\text{C y}^{-1}$, $p < 0.01$) present the
233 highest increasing trend, i.e., both months experienced ca. $+2.1 \text{ } ^\circ\text{C}$ over thirty years (Fig.
234 5c). The cold season experienced a positive trend ($0.046 \pm 0.012 \text{ } ^\circ\text{C y}^{-1}$, $p < 0.01$) mainly
235 concentrated in the post-monsoon period. As highlighted by the progressive $\mu(\tau)$ trend
236 in the bottom graph (full line in blue), this trend started increasing in 2005. In the warm
237 season, the trend is much lower ($0.024 \pm 0.014 \text{ } ^\circ\text{C y}^{-1}$, $p < 0.1$) and it is negative in May.
238 On the annual scale the trend is moderately negative ($-0.030 \pm 0.009 \text{ } ^\circ\text{C y}^{-1}$, $p > 0.01$).

239 *Mean air temperature (Tmean)*

240 Figure 5b presents, as expected, intermediate conditions for Tmean. The cold season
241 shows increasing trends, although not significant ($0.020 \pm 0.009 \text{ } ^\circ\text{C y}^{-1}$, $p > 0.1$), and only
242 November and December significantly rise. In the warm season, there is no trend ($0.003 \pm$
243 $0.010 \text{ } ^\circ\text{C y}^{-1}$, $p > 0.1$), while the temperature in May decreases. Also considering the
244 annual scale, there is no trend in the last 30 years ($0.005 \pm 0.007 \text{ } ^\circ\text{C y}^{-1}$, $p > 0.1$).

245 *Total precipitation (Prec)*

246 In the last years, for all months of the warm season, an overall and strongly significant
247 decreasing trend of Prec has occurred (Fig. 5d). Considering all period, a continuous
248 decreasing trend has occurred since 2000, which became significant at the beginning of
249 2005. The decreasing Prec trend is highest in August. During the warm season, the
250 reduction of precipitation has been 41%.



251

252 **Conclusion**

253 Glaciers in the Himalaya are a major focus of international research, for their relevance
254 for water and people, their role in climate-land feedbacks and their iconic and not entirely
255 understood patterns of changes. One of the major drawbacks in Himalayan research of
256 the cryosphere is that there are almost no long-term climate measurements at high
257 elevations, where glaciers are located. Here, we presented station data of 7 stations
258 belonging to the Pyramid Meteorological Network managed by EV-K2-CNR.

259 Moreover, we presented the precipitation and temperature time series based on a three-
260 decade effort to ensure a continuous monitoring of the high-elevation climate in the
261 Himalaya.

262 Strikingly, our measurements reveal a local cooling at glacierized elevations which is
263 in stark contrast to the postulated temperature increases. An interpretation of this
264 phenomenon was provided recently by Salerno et al., 2023. What is interesting here is to
265 highlight that by means of this unique data and the perseverance of the measurements it
266 has made it possible to tell a story that goes against the trend of current knowledge based
267 on data collected elsewhere or at low altitude.

268 We are convinced that making this data available will open new perspectives on
269 climate change and its effects in the Himalaya that will guide research at high elevations
270 in the coming decades

271 **Data availability**

272 All datasets described and presented in this paper can be openly accessed from
273 <https://geoportal.mountaingenius.org/portal/>. Moreover, the dataset is accessed from
274 <https://zenodo.org/records/14450214> (Salerno et al., 2024) and distributed under the
275 CCBY4.0 license.

276 **Competing interests**

277 The authors declare that they have no conflict of interest.

278 **Special issue statement**



279 This article is part of the special issue “Hydrometeorological data from mountain and
280 alpine research catchments”. It is not associated with a conference.

281 **Author contribution**

282 F.S., N.G. and N.C. drafted the article, G. T. contributed to improving the manuscript,
283 M.T.M. and F. D. built the Geonetwork platform, N.G. assured the data quality assess-
284 ment, G. V. and K. B. are the responsible for the management of the weather stations.

285 **Acknowledgements**

286 The Pyramid Meteorological Network was supported by the MIUR (Ministero
287 dell'Istruzione e del Merito) through Ev-K2-CNR/SHARE and CNR-DTA/NEXTDATA
288 project within the framework of the Ev-K2-CNR and Nepal Academy of Science and
289 Technology (NAST).

290 **References**

- 291 Abebe, A., Solomatine, D., and Venneker, R.: Application of adaptive fuzzy rule based
292 models for reconstruction of missing precipitation events, *Hydrolog. Sci. J.*, 45, 425–
293 436, <https://doi.org/https://doi.org/10.1080/02626660009492339>, 2000.
294 <https://doi.org/>
- 295 Abudu, S., Bawazir, A. S., and King, J. P.: Infilling missing daily evapotranspiration data
296 using neural networks, *J. Irrig. Drain. E-asce*, 136, 317–325,
297 [https://doi.org/https://doi.org/10.1061/\(ASCE\)IR.1943-4774.0000197](https://doi.org/https://doi.org/10.1061/(ASCE)IR.1943-4774.0000197), 2010.
- 298 Amatya, L. K., Cuccillato, E., Haack, B., Shadie, P., Sattar, N., Bajracharya, B., Shrestha,
299 B. Caroli, P., Panzeri, D., Basani, M., Schommer, B., Flury, B. Salerno, F., and
300 Manfredi, E. C.: Improving communication for management of social-ecological
301 systems in high mountain areas: Development of methodologies and tools – The
302 HKKH Partnership Project, *Mt. Res. Dev.*, 30, 69-79,
303 <https://doi.org/https://doi.org/10.1659/MRD-JOURNAL-D-09-00084.1>, 2010.
- 304 Bertolani L., Bollasina, M., and Tartari, G.: Recent biannual variability of meteorological
305 features in the Eastern Highland Himalayas, *Geophys. Res. Lett.*, 27, 2185-2188,
306 <https://doi.org/https://doi.org/10.1029/1999GL011198>, 2000.
- 307 Bhattacharya, A., Bolch, T., Mukherjee, K., King, O., Menounos, B., Kapitsa, V., ... and
308 Yao, T.: High Mountain Asian glacier response to climate revealed by multi-temporal
309 satellite observations since the 1960s. *Nature Commun.*, 12(1), 4133.,
310 <https://doi.org/10.1038/s41467-021-24180-y>, 2021.
- 311 Bhuju, D. R., Carrer, M., Gaire, N. P., Soraruf, L., Riondato, R., Salerno, F., & Maharjan,
312 S. R.: Dendroecological study of high altitude forest at Sagarmatha National Park,



313 Nepal. Contemporary research in Sagarmatha (Mt. Everest) region, Nepal, 119-130,
314 2010.

315 Biemans, H., Siderius, C., Lutz, A. F., Nepal, S., Ahmad, B., Hassan, T., ... and Immerzeel,
316 W. W.: Importance of snow and glacier meltwater for agriculture on the Indo-Gangetic
317 Plain. *Nat. Sustain.*, 2(7), 594-601, <https://doi.org/10.1038/s41893-019-0305-3>, 2019.

318 Bocchiola, D. and Diolaiuti, G.: Evidence of climate change within the Adamello Glacier
319 of Italy, *Theor. Appl. Climatol.*, 100, 351–369, <https://doi.org/10.1007/s00704-009-0186-x>, 2010.

321 Coulibaly, P. and Evora, N.: Comparison of neural network methods for infilling missing
322 daily weather records, *J. Hydrol.*, 341, 27–41,
323 <https://doi.org/10.1016/j.jhydrol.2007.04.020>, 2007.

324 Déqué, M.: Frequency of precipitation and temperature extremes over France in an
325 anthropogenic scenario: model results and statistical correction according to observed
326 values, *Global Planet. Change*, 57, 16–26,
327 <https://doi.org/10.1016/j.gloplacha.2006.11.030>, 2007.

328 Gerstengarbe, F. W. and Werner, P. C.: Estimation of the beginning and end of recurrent
329 events within a climate regime, *Clim. Res.*, 11, 97-107,
330 <https://doi.org/10.3354/cr011097>, 1999.

331 Guyennon, N., Romano, E., Portoghese, I., Salerno, F., Calmanti, S., Petrangeli, A. B.,
332 Tartari, G., and Copetti, D.: Benefits from using combined dynamical-statistical
333 downscaling approaches – lessons from a case study in the Mediterranean region,
334 *Hydrol. Earth Syst. Sc.*, 17, 705–720, <https://doi.org/10.5194/hess-17-705-2013>, 2013.

335 Ichiyanagi, K., Yamanaka, M. D., Muraji, Y., and Vaidya, B. K.: Precipitation in Nepal
336 between 1987 and 1996, *Int. J. Climatol.*, 27, 1753–1762,
337 <https://doi.org/10.1002/joc.1492>, 2007.

338 James, A. L. and Oldenburg, C. M.: Linear and Monte Carlo uncertainty analysis for
339 subsurface contaminant transport simulation, *Water Resour. Res.*, 33, 2495–2508,
340 <https://doi.org/10.1029/97WR01925>, 1997.

341 Kattel, D. B. and Yao, T.: Recent temperature trends at mountain stations on the southern
342 slope of the central Himalayas, *J. Earth Syst. Sci.*, 122, 215–227, <https://doi.org/10.1007/s12040-012-0257-8>, 2013.

344 Kattel, D. B., Yao, T., Yang, K., Tian, L., Yang, G. and Joswiak, D.: Temperature lapse
345 rate in complex mountain terrain on the southern slope of the central Himalayas, *Theor.*
346 *Appl. Climatol.*, 113, 671-682, <https://doi.org/10.1007/s00704-012-0816-6>, 2013.

347 Kendall, M.G.: *Rank Correlation Methods*, Oxford University Press, New York, 1975.

348 Lin, C., Yang, K., Chen, D., Guyennon, N., Balestrini, R., Yang, X., ... and Salerno, F.:
349 Summer afternoon precipitation associated with wind convergence near the Himalayan
350 glacier fronts. *Atmospheric Research*, 259, 105658,
351 <https://doi.org/10.1016/j.atmosres.2021.105658>, 2021.

352 Locci, F., Melis, M.T., Dessì, F., Stocchi, P., Akinde, M.O., Bønes, V., Bonasoni, P., and Vuiller-
353 moz, E.: Implementation of a webGIS service platform for high mountain climate research:
354 the SHARE GeoNetwork project. *Geosci. Data J.*, 1: 140-157. <https://doi.org/10.1002/gdj3.14>,
355 2014.



- 356 Magnani, A., Ajmone-Marsan, F., D'Amico, M., Balestrini, R., Viviano, G., Salerno, F.,
357 and Freppaz, M.: Soil properties and trace elements distribution along an altitudinal
358 gradient on the southern slope of Mt. Everest, Nepal. *Catena*, 162, 61-71,
359 <https://doi.org/10.1016/j.catena.2017.11.015>, 2018.
- 360 Matthews, T., Perry, L. B., Koch, I., Aryal, D., Khadka, A., Shrestha, D., ... and Mayewski,
361 P. A.: Going to extremes: installing the world's highest weather stations on Mount
362 Everest. *Bull. Am. Meteorol. Soc.*, 101(11), E1870-E1890,
363 <https://doi.org/10.1175/BAMS-D-19-0198.1>, 2020.
- 364 Melis M. T., Dessi F., Locci F., Bonasoni P. and Vuillermoz E.: Share Geonetwork: a web-service
365 platform for environmental data sharing, Proc. SPIE 8795, First International Conference on
366 Remote Sensing and Geoinformation of the Environment (RSCy2013), 87951V (August 5,
367 2013); <https://doi.org/10.1117/12.2027602>. 2013.
- 368 Mountain Research Initiative EDW Working Group: Elevation-dependent warming in
369 mountain regions of the world. *Nature Clim Change* **5**, 424-430
370 <https://doi.org/10.1038/nclimate2563>, 2015.
- 371 Pandey, J., Sigdel, S. R., Lu, X., Salerno, F., Dawadi, B., Liang, E., & Camarero, J. J.:
372 Early growing-season precipitation drives radial growth of alpine juniper shrubs in the
373 central Himalayas. *Geografiska annaler: series a, physical geography*, 102(3), 317-
374 330, <https://doi.org/10.1080/04353676.2020.1761097>, 2020.
- 375 Potter, E. R., Orr, A., Willis, I. C., Bannister, D., & Salerno, F.: Dynamical drivers of the
376 local wind regime in a Himalayan valley. *J. Geophys. Res. Atmos.* 123(23), 13-186,
377 <https://doi.org/10.1029/2018JD029427>, 2018.
- 378 Salerno, F., Cuccillato, E., Caroli, P., Bajracharya, B., Manfredi, E. C., Viviano, G.,
379 Thakuri, S., Flury, B., Basani, M., Giannino, F., and Panzeri, D.: Experience with a
380 hard and soft participatory modeling framework for social ecological system manage-
381 ment in Mount Everest (Nepal) and K2 (Pakistan) protected areas, *Mt. Res. Dev.*, 30,
382 80-93, <https://doi.org/10.1659/MRD-JOURNAL-D-10-00014.1>, 2010.
- 383 Salerno, F., Guyennon, N., Thakuri, S., Viviano, G., Romano, E., Vuillermoz, E., ... and
384 Tartari, G.: Weak precipitation, warm winters and springs impact glaciers of south
385 slopes of Mt. Everest (central Himalaya) in the last 2 decades (1994–2013). *The*
386 *Cryosphere*, 9(3), 1229-1247, <https://doi.org/10.5194/tc-9-1229-2015>, 2015.
- 387 Salerno, F., Guyennon, N., Yang, K., Shaw, T. E., Lin, C., Colombo, N., ... and Pellicciotti,
388 F.: Local cooling and drying induced by Himalayan glaciers under global
389 warming. *Nat. Geosci.*, 16(12), 1120-1127, [https://doi.org/10.1038/s41561-023-](https://doi.org/10.1038/s41561-023-01331-y)
390 01331-y, 2023.
- 391 Salerno, F., Thakuri, S., Tartari, G., Nuimura, T., Sunako, S., Sakai, A., and Fujita, K.:
392 Debris-covered glacier anomaly? Morphological factors controlling changes in the
393 mass balance, surface area, terminus position, and snow line altitude of Himalayan
394 glaciers. *Earth Planet. Sci. Lett.*, 471, 19-31,
395 <https://doi.org/10.1016/j.epsl.2017.04.039>, 2017.
- 396 Salerno, F., Guyennon, N., Colombo, N., Melis, M. T., Dessi, F. G., Verza, G., Bista, K.,
397 Sheharyar, A., and Tartari, G. (2024). Pyramid Meteorological Network - EVK2CNR
398 (Version 1) [Data set]. Zenodo <https://zenodo.org/records/14450214>.



- 399 Schneider, T.: Analysis of incomplete climate data: Estimation of mean values and
400 covariance matrices and imputation of missing values, *J. Clim.*, 14, 853–871,
401 [https://doi.org/10.1175/1520-0442\(2001\)014<0853:AOICDE>2.0.CO;2](https://doi.org/10.1175/1520-0442(2001)014<0853:AOICDE>2.0.CO;2), 2001.
- 402 Sen, P. K.: Estimates of the regression coefficient based on Kendall’s Tau, *J. Am. Assoc.*,
403 63, 1379-1389, <https://doi.org/10.2307/2285891>, 1968.
- 404 Shea, J. M., Immerzeel, W. W., Wagnon, P., Vincent, C., & Bajracharya, S.: Modelling glacier
405 change in the Everest region, Nepal Himalaya. *The Cryosphere*, 9(3), 1105-1128.,
406 <https://doi.org/10.5194/tc-9-1105-2015>, 2015.
- 407 Shrestha, A. B., Wake, C. P., Mayewski, P. A., and Dibb, J. E.: Maximum temperature
408 trends in the Himalaya and its vicinity: An analysis based on temperature records from
409 Nepal for the period 1971-94, *J. Clim.*, 12, 2775-5561, [https://doi.org/10.1175/1520-0442\(1999\)012<2775:MTTITH>2.0.CO;2](https://doi.org/10.1175/1520-0442(1999)012<2775:MTTITH>2.0.CO;2), 1999.
- 411 Sigdel, S. R., Pandey, J., Liang, E., Muhammad, S., Babst, F., Leavitt, S. W., ... and
412 Peñuelas, J.: No benefits from warming even for subnival vegetation in the central
413 Himalayas. *Sci Bull*, 66(18), 1825-1829, 2021.
- 414 Tartari, G., Salerno, F., Buraschi, E., Bruccoleri, G., and Smiraglia, C.: Lake surface area
415 variations in the North-Eastern sector of Sagarmatha National Park (Nepal) at the end
416 of the 20th Century by comparison of historical maps, *J. Limnol.*, 67, 139-154,
417 <https://doi.org/10.4081/jlimnol.2008.139>, 2008.
- 418 Thakuri, S., Salerno, F., Bolch, T., Guyennon, N., & Tartari, G.: Factors controlling the
419 accelerated expansion of Imja Lake, Mount Everest region, Nepal. *Ann. Glaciol.*, 57(71), 245-257., 2016.
- 421 Thakuri, S., Salerno, F., Smiraglia, C., Bolch, T., D’Agata, C., Viviano, G., and Tartari,
422 G.: Tracing glacier changes since the 1960s on the south slope of Mt. Everest (central
423 southern Himalaya) using optical satellite imagery, *The Cryosphere*, 8, 1297-1315,
424 <https://doi.org/10.5194/tc-8-1297-2014>, 2014.
- 425 Themeßl, M. J., Gobiet, A., and Heinrich, G.: Empirical-statistical downscaling and error
426 correction of regional climate models and its impact on the climate change signal,
427 *Climatic Change*, 112, 449-468, <https://doi.org/10.1007/s10584-011-011-0224-4>,
428 2012.
- 429 Yang, K., Guyennon, N., Ouyang, L., Tian, L., Tartari, G., and Salerno, F.: Impact of
430 summer monsoon on the elevation-dependence of meteorological variables in the
431 south of central Himalaya. *International J.Clim.*, 38(4), 1748-1759,
432 <https://doi.org/10.1002/joc.5293>, 2018.
- 433 Yao, T., Bolch, T., Chen, D., Gao, J., Immerzeel, W., Piao, S., ... and Zhao, P.: The
434 imbalance of the Asian water tower. *Nat. Rev. Earth Environ.*, 3(10), 618-632,
435 <https://doi.org/10.1038/s43017-022-00299-4>, 2022.
- 436 Wagnon, P., Brun, F., Khadka, A., Berthier, E., Shrestha, D., Vincent, C., ... and Jomelli,
437 V.: Reanalysing the 2007–19 glaciological mass-balance series of Mera Glacier,
438 Nepal, Central Himalaya, using geodetic mass balance. *J.Glaciol.*, 67(261), 117-125,
439 <https://doi.org/10.1017/jog.2020.88>, 2021.
- 440



441 *Table 1. List of surface stations belonging to Pyramid Meteorological Network*

Station ID	Location	Latitude °N	Longitude °E	Elevation m a.s.l.	Mean feature of the landscape	Sampling rate
AWSSC	South Col	27.98	86.76	7 986	Mountain peak (off glacier)	1 hour
CNG_SNP	Changri Nup	27.96	86.93	5 700	Glacier (on glacier)	1 hour
AWS4	Kala Patthar	27.99	86.83	5 600	Mean glaciers surface (on glacier)	1 hour
AWS0, AWS1	Pyramid	27.96	86.81	5 035	Mean glacier fronts (off glacier)	1 hour
AWS2	Pheriche	27.90	86.82	4 260	Treeline (off glacier)	1 hour
AWS5	Namche	27.80	86.71	3 570	Forests (off glacier)	1 hour
AWS3	Lukla	27.70	86.72	2 660	Forests (off glacier)	1 hour

442

443 *Table 2. % of daily missing data for each variable. AT: 2m Atmospheric Temperature*
 444 *(°C); RR: Rainfall Rate (mm); RH: Relative Humidity (%); AP: Atmospheric Pressure*
 445 *(hPa); WS: Wind Speed (m/s); WD: Wind Direction (°)*

446

Missing rate (1994/2023) (%)	AP	AT	RH	RR	WD	WS	UVA
Z7986	54	61.8	78	-	67.9	64.9	46,6
Z5700	-	6	6	-	25.6	25.1	-
Z5600	16.5	18.1	18.9	44.6	26.9	28.2	-
Z5035 (AWS0)	12.6	18.1	18.5	23.3	53.4	12.6	-
Z5035 (AWS1)	7.2	6.8	22.3	9.4	10.5	9.1	-
Z4260	13	15.3	14.4	14.8	20.2	23.3	-
Z3570	39	41.9	53.1	42.9	43.7	42.5	-
Z2660	49.1	51	63	52.1	54	49.4	-

447

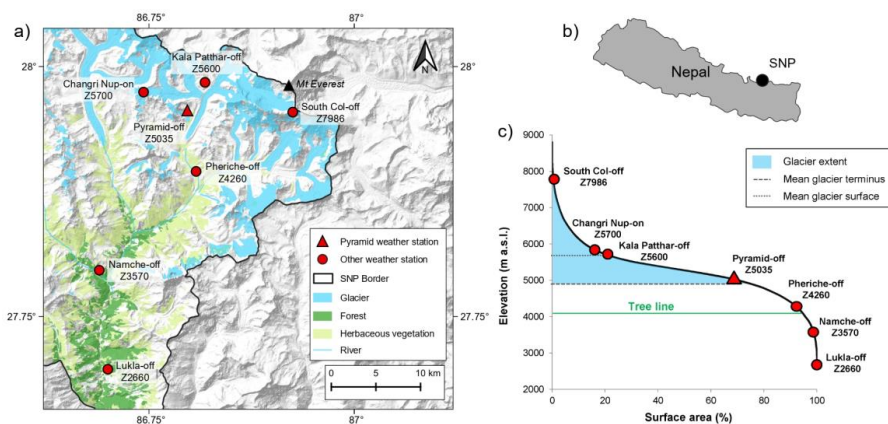
448 *Table 3. List of sensors with measurement height, manufacturer and accuracy.*

Parameter	Sensor	Manufacturer	Accuracy
Air temperature	AWS0 (Z5035) Precision Linear Thermistor (2m)	MTX	0.1°C



Precipitation	Tipping Bucket (1.5m)	MTX	0.2 mm
Relative humidity	Solid state hygrometer (2m)	MTX	3%
Atmospheric pressure	Aneroid capsule (2m)	MTX	0.5hPa
AWS1(Z5035)			
Air temperature	Thermoresistance (2m)	Lsi-Lastem	0.1°C
Precipitation	Tipping Bucket (1.5m)	Lsi-Lastem	2%
Relative humidity	Capacitive Plate (2m)	Lsi-Lastem	2.5%
Atmospheric pressure	Slice of Silica (2m)	Lsi-Lastem	1hPa
AWS4(Z5035)			
Air temperature	Thermoresistance (2m)	Lsi-Lastem	0.1°C
Precipitation	Tipping Bucket (1.5m)	Lsi-Lastem	1%
Relative humidity	Capacitive Plate (2m)	Lsi-Lastem	1.5%
Atmospheric pressure	Slice of Silica (2m)	Lsi-Lastem	1hPa
AWS2(Z4260)			
Air temperature	Thermoresistance (2m)	Lsi-Lastem /Vaisala	0.1°C/0.3°C
Precipitation	Tipping Bucket (1.5m)	Lsi-Lastem	2%
Relative humidity	Capacitive Plate (2m)	Lsi-Lastem /Vaisala	1.5%/2.5%
Atmospheric pressure	Slice of Silica (2m)	Lsi-Lastem /Vaisala	1hPa/0.5 hPa
AWS5(Z3570)			
Air temperature	Thermoresistance (2m)	Lsi-Lastem	0.1°C
Precipitation	Tipping Bucket (1.5m)	Lsi-Lastem	2%
Relative humidity	Capacitive Plate (2m)	Lsi-Lastem	2.50%
Atmospheric pressure	Slice of Silica (2m)	Lsi-Lastem	1hPa
AWS3(Z2660)			
Air temperature	Thermoresistance (2m)	Lsi-Lastem /Vaisala	0.1°C/0.3°C
Precipitation	Tipping Bucket (1.5m)	Lsi-Lastem	2%
Relative humidity	Capacitive Plate (2m)	Lsi-Lastem /Vaisala	1.5%/2.5%
Atmospheric pressure	Slice of Silica (2m)	Lsi-Lastem /Vaisala	1hPa/0.5 hPa
CNG_SNP(Z5700)			
Air temperature	Thermoresistance (2m)	Lsi-Lastem /Vaisala	0.1°C/0.3°C
Precipitation	Tipping Bucket (1.5m)	Lsi-Lastem	2%
Relative humidity	Capacitive Plate (2m)	Lsi-Lastem /Vaisala	1.5%/2.5%
Atmospheric pressure	Slice of Silica (2m)	Lsi-Lastem /Vaisala	1hPa/0.5 hPa
AWSSC(Z7986)			
Air temperature	Thermoresistance (2m)	Lsi-Lastem /Vaisala	0.1°C/0.3°C
Precipitation	Tipping Bucket (1.5m)	Lsi-Lastem	2%
Relative humidity	Capacitive Plate (2m)	Lsi-Lastem /Vaisala	1.5%/2.5%
Atmospheric pressure	Slice of Silica (2m)	Lsi-Lastem /Vaisala	1hPa/0.5 hPa

449



450

451 *Figure 1. a, b) Location of meteorological monitoring network in the Sagarmatha*
 452 *National Park (SNP), Nepal c) Hypsometric curve of SNP and altitudinal glacier*
 453 *distribution. Along this curve, the locations of meteorological stations belonging to*
 454 *Pyramid Observatory Laboratory are presented.*



455

456



457

458 *Figure 2. Photographs of the Pyramid Meteorological Network*

459

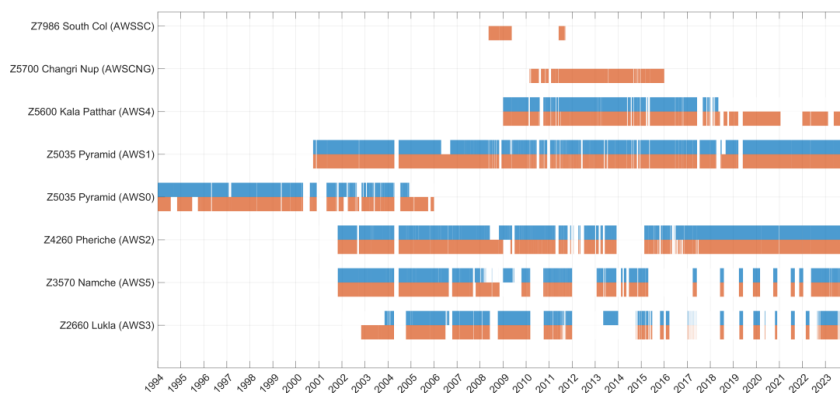
460

461



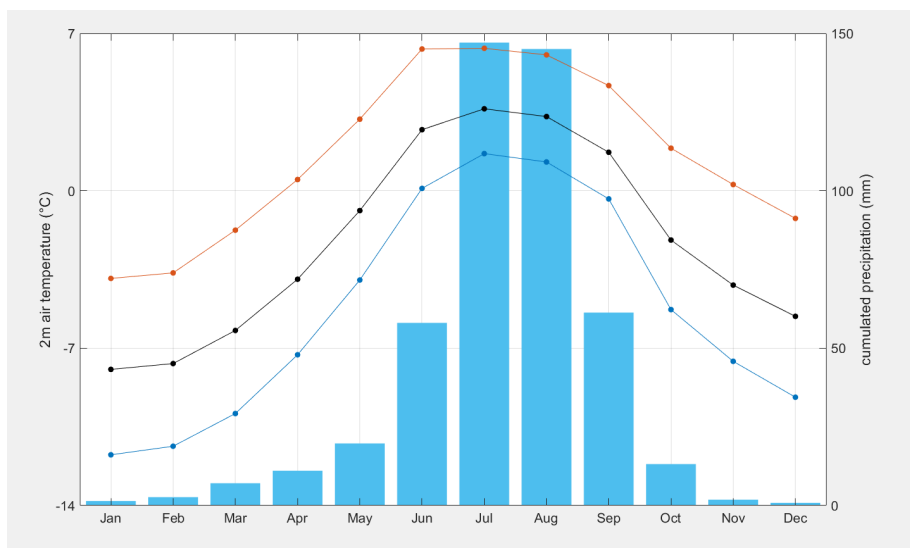
462

463



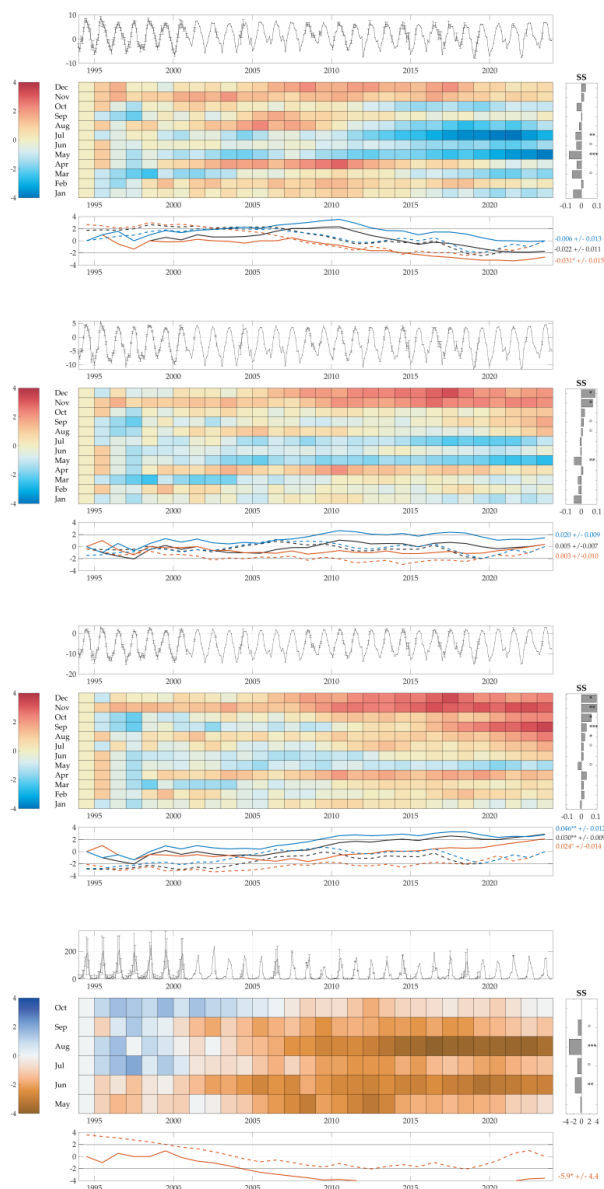
464

465 *Figure 3. Available data time series (precipitation: blue; temperature: orange) for the*
466 *Pyramid Meteorological Network since 1994*



467

468 *Figure 4. Mean monthly cumulated precipitation and minimum, maximum, and mean*
469 *temperature at Pyramid station (Z5035 m a.s.l. reference period 1994–2023).*



470

471 *Figure 5. Air temperature and precipitation trend analysis at Pyramid station (Z5035).*
472 *Complete time series for a) maximum, b) mean, c) minimum, and d) total precipitation.*
473 *The top graph of each meteorological variable (from a to d) shows the monthly trend. The*
474 *grids display the results of the MK test applied at the monthly scale and calculated from*
475 *the beginning of the series to the given year. The colour bar represents the normalized*
476 *Kendall's tau coefficient $\mu(\tau)$. The colour tones below -1.96 and above 1.96 are*



477 significant ($\alpha = 5\%$). On the right, the monthly Sen's Slope (SS) and the significance levels
478 for 1994–2023 ($P < 0.1$, $*P < 0.05$, $**P < 0.01$, $***P < 0.001$). The bottom graph plots
479 the progressive $\mu(\tau)$ (solid lines) and retrograde (dotted line) of the seqMK test (that is,
480 calculated from the beginning or from the end, respectively, of the series to the given year)
481 for the cold season (NDJFMA) (blue), the warm season (MJJASO) (orange) and for the
482 entire year (black). For each year, below-zero lines indicate negative trends (calculated
483 from 1994).